Available online at www.sciencedirect.com
ScienceDirect
Journal of Sound and Vibration 309 (2008) 677–694
JOURNAL OF SOUND AND VIBRATION
www.elsevier.com/locate/jsvi

Actuation of a discontinuous structure with piezoelectric actuators

Jingdou Wang[a], W. Steve Shepard Jr.[a,*], Kenneth A. Cunefare[b], Keith A. Williams[a]

[a]*Department of Mechanical Engineering, University of Alabama, 290 Hardaway Hall, P.O. Box 870276, Tuscaloosa, AL 35487, USA*
[b]*Georgia Institute of Technology, George W. Woodruff School of Mechanical Engineering, 801 Ferst Drive N.W., Atlanta, GA 30332-0405, USA*

Received 9 March 2006; received in revised form 19 April 2007; accepted 26 July 2007
Available online 24 October 2007

Abstract

An alternate approach to exciting a one-dimensional structure with discontinuities using a piezoelectric actuator is presented and examined. Instead of being bonded to the uniform side of a beam, the piezoelectric actuator is attached such that it spans two adjacent rib discontinuities. In this configuration, the actuator generates an eccentric actuation force on the structure and induces both axial and transverse motions. The goal of this work is to first model the axial and transverse response caused by the piezoelectric actuator. Then, the change in that response is examined for the case where an external disturbance force is present. The system is modeled by coupling the piezoelectric strain and structural dynamic response. The characteristics of the voltage-generated piezoelectric forces are discussed through numerical examples. The structural response found using the dynamic force–voltage model for the actuator is then compared to the response when the actuator model is approximated by its static or zero-frequency value. Furthermore, the ability of the actuator to potentially provide better control authority by using this alternate configuration is examined. The numerical study shows that when the actuator spans two discontinuities, there is potential for greater control authority than when that same actuator is placed on the uniform side of the structure.

1. Introduction

Active vibration control of beam-like structures using surface-bonded piezoelectric actuators has been extensively studied. Early work by Crawley and de Luis [1] demonstrated the effective use of piezoelectric actuators in controlling beam vibrations. In their work, Crawley and de Luis analyzed the stresses, strains, and loads generated on a one-dimensional (1-D) cantilevered beam by piezoelectric actuator pairs bonded symmetrically on both sides of the beam or embedded in the beam structure. Their research showed that, in the limiting case when the bonding layers between the actuator and structure are infinitely thin and stiff, the excitation from the piezoelectric actuators acts as two line moments concentrated at the two ends of the actuators. Clark et al. [2] developed a theoretical model to predict the response of a simply supported beam

*Corresponding author. Tel.: +1 205 348 0048; fax: +1 205 348 6419.
E-mail address: sshepard@eng.ua.edu (W. Steve Shepard Jr.).

0022-460X/$ - see front matter © 2007 Elsevier Ltd. All rights reserved.
doi:10.1016/j.jsv.2007.07.082

excited by multiple pairs of piezoelectric actuators. Their work demonstrated the use of multiple independent actuators to excite particular modes. Clark et al. [2] also conducted experiments and compared the experimental and theoretical results. Further modeling work was done by Dimitriadis et al. [3] who examined the case of piezoelectric actuation pairs symmetrically bonded on a 2-D plate. In that work, the induced actuation moments were determined and the modal responses were compared for different actuator locations.

While symmetric bonding of actuators on the upper and lower surfaces of a structure can be used to induce pure bending moments in the structure, a single piezoelectric actuator simultaneously excites both extensional and flexural motions in a structure, as shown by Gibbs and Fuller [4]. An analytical model for a single piezoelectric element bonded on the surface of a thin long beam was developed by those authors. The results showed that a single actuator is mathematically equivalent to a combination of moments and in-plane forces located at the ends of the actuator. Using a similar approach, the 1-D piezoelectric asymmetric excitation model was extended to a 2-D plate vibration excitation model [5]. In that work, the induced distributed moments in the both x- and y-directions were determined.

In the works described above, the induced actuation strains in the underlying structures were found using static approaches. That is, the relationship between the applied voltage across the actuator thickness and the resulting structural strain was formulated from an assumption of static equilibrium and the compatibility equations [6]. Pan, Hansen, and Synder [7] developed a dynamic model for a simply supported beam with a piezoelectric actuator pair bonded on the surface. Through solving the coupled dynamic equations of the beam and the actuators, it was shown that, in order to obtain an accurate description of the strain field in the structure, the coupled structural and piezoelectric actuator system should be modeled using a dynamic approach. This was shown to be especially true for strains in the vicinity of the actuator.

Proper selection of actuator locations can be a critical issue when exciting or controlling a particular vibration mode. Crawley et al. [1] found that, in order to excite a specific mode effectively, the actuator should be placed in regions of high average strains for that mode and away from zero strains. The optimal size and location of a piezoelectric actuator pair symmetrically bonded on a beam with arbitrary boundary conditions were studied based on the modal cost and controllability index [8]. It is important to note that, in many cases, actuators cannot be arbitrarily placed. For the study discussed in Ref. [5], the controlled structure of interest was a simulated rack shelf used on International Space Station (ISS). On ISS, the laboratory experiments are conducted in different experiment racks. In each rack, shelves are used to support an experiment. To reduce weight, the top of the shelf surface is uniformly flat while most of the material on the opposite side is removed to leave a waffle-like pattern of supporting ribs. To use active methods to reduce vibrations of the simulated shelf, in that research, the actuators were placed in a typical manner to the uniform side of the shelf. However, in practice, it may not be practical to mount the actuators on the uniform side of the shelf, as that side will be taken up by items needed to operate the experiment. As such, it would be better from a logistical standpoint to place the actuators on the side of the shelf with the waffle-like pattern. At the same time, the existence of the ribs may present an opportunity to try an alternative approach to vibration control: mounting the piezoelectric actuators at the ends of and between adjacent ribs.

As an extension of Ref. [5], which considered conventional actuator placement, this paper examines a new perspective for actuator placement and actuator-structure modeling: instead of placing the actuator on the uniform side of the structure, the piezoelectric actuator will be placed on the ribbed side of the structure, as shown in Fig. 1(a) and (b). In Fig. 1(a), the primary input of the system is the external disturbance force, f_p, and the secondary (control) input comes from the actuator. The actuator spans the gap between two of the ribs. In other words, the actuators are to be mounted on the side of a structure that contains significant discontinuities. One of the motivations for considering this configuration is the potential for greater dynamic control authority by the actuator, due to the actuator's placement at a larger distance from the neutral axis of the underlying structure. When a voltage is applied to the piezoelectric patch bonded across the ribs, the patch attempts to expand or contract. However, this change of length is partially constrained by the stiffness of the rib discontinuities and the base structure. As a result, under the assumption that no buckling occurs in the piezoelectric actuator, the actuator will generate two equal and opposite forces on the edges of the ribs, as shown in Fig. 1(b). At the same time, placing the actuator in such a configuration will impact the excitation characteristics and actuator's control authority. In this initial study, which is intended to examine potential benefits of an alternative control approach, issues associated with the packaging requirements for this

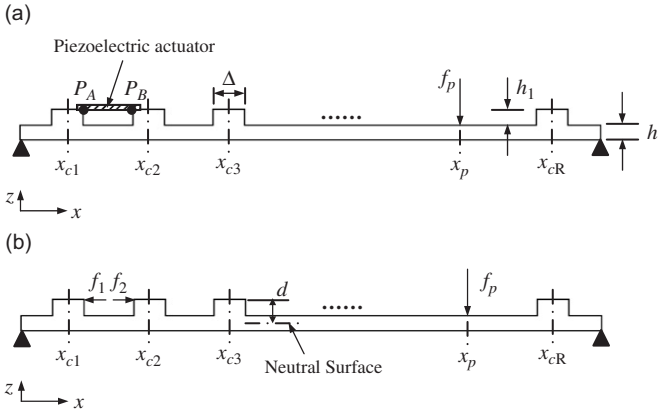

Fig. 1. Piezoelectric actuator on a one-dimensional discontinuous structure: (a) piezoelectric actuator spanning the rib discontinuities and (b) equal and opposite piezoelectric forces acting on the discontinuities.

piezoceramic actuator configuration are not considered, although potential solutions to this issue have been examined previously [9]. It is assumed that the actuator has sufficient structural integrity to operate in this configuration. A more detailed study of those packaging requirements along with their impact on the actuator modeling will be the subject of future research. The axial actuation loads on the tips of the ribs will generate bending moments on the beam due to the actuator's eccentricity relative to the structural neutral surface. Since the actuator is farther from the neutral axis in this case than when mounted on the uniform side, there is the potential to generate larger flexural moments. It is important to note that the piezoelectric strain and force are related to both the transverse and axial vibrations in the beam structure. As a result, vibrations in both of these directions will be modeled. The control authority of this approach is influenced by several factors, including actuator position and the geometric properties of the discontinuities, like the rib height. One of the objectives of this work is to examine the impact of some of these parameters on the actuator's dynamic control authority. Prior to that study, though, the relationship between the actuator voltage and the resulting structural stress and strain will be addressed.

In the following sections, an analytical model is developed to describe the dynamics of an actuator that is mounted such that it spans two adjacent rib discontinuities. This work initially formulates this model from a dynamic standpoint. The ability of a low-frequency description (i.e. $\omega = 0$) to adequately represent that model is then examined, to determine situations where the complexity of the full dynamic model is not needed and the linearized approach may be sufficient. In addition to verifying some of the analytical modeling via numerical models implemented using the finite element (FE) method, the impact of some of the important structural characteristics on the control authority of the actuator is also examined. Note that the non-ideal strain and the hysteresis properties of the piezoceramics described in Ref. [10] are not considered in this research.

2. System modeling

A sketch of the beam with multiple rib discontinuities to be considered is shown in Fig. 1(a). The length of the beam is L. The width and thickness of the beam are b and h, the height of the ribs is given by h_1, the center locations of the ribs are x_{ci} ($i = 1, 2, \ldots, R$). Note that the ribs are not uniformly spaced. For simplicity, the lengths of all the ribs are equal and given by Δ. In addition, it is assumed that the ribs extend the full width of the beam. A piezoelectric actuator is bonded such that it spans two adjacent ribs as shown in Fig. 1(a). As mentioned earlier, it is assumed that the actuator can be encapsulated to operate in this configuration. Due to the eccentric position of the actuation forces on the ribs, both transverse and axial vibrations will be induced in the beam. The actual piezoelectric strain is determined by the applied voltage as well as the axial displacement at the tips of the two ribs. This displacement will be due to both the transverse and axial

vibration of the beam. Therefore, to obtain the piezoelectric actuator strain, actuator motions caused by both axial and transverse beam vibrations are considered in this work.

In this section, models for the transverse and axial forced vibrations are first developed. The piezoelectric strain and the structural dynamic response are coupled in order to determine the piezoelectric actuation force and the structure strain. Furthermore, the effect of including the external disturbance force on the piezoelectric actuation forces is investigated.

2.1. Modeling the forced vibration of a ribbed beam

The actuator generates two equal and opposite forces on the edges of the ribs. The transverse and axial dynamic response of a ribbed beam due to the two harmonic forces caused by the actuator, as shown in Fig. 1(b), are predicted using the Ritz expansion method and Lagrange's Equations. Note that while the external disturbance force, f_p, is present in the figure, it is not considered until a later section. First, for transverse and axial vibrations, the kinetic and potential energy expressions for the structure are determined. In this model, both the stiffness and inertia of the ribs are considered. The generalized force is then formulated based on the virtual work resulting from the two point forces acting at the tips of the ribs. By solving the eigenvalue problem for the unforced structure, the natural frequencies and modal shapes of the structure can be determined. The dynamic response can then be expressed through a modal superposition. One of the intentions of this initial study is to determine if further study of this configuration is warranted by potential improvements in performance. To simplify this initial study, it is assumed that the transverse and axial vibrations are uncoupled. The transverse forced vibration will be modeled first.

The transverse displacement of the beam is expressed by an N_1-term Ritz expansion

$$w(x,t)=\sum_{j=1}^{N_1}\phi_j(x)q_j(t),\quad 0\leqslant x\leqslant L, \tag{1}$$

where ϕ_j are the basis functions which satisfy the transverse geometric boundary conditions and q_j are the generalized coordinates. The generalized coordinates are assumed to have a harmonic time dependency, given by

$$q_j=\mathrm{Re}[W_j\,\mathrm{e}^{\mathrm{i}\omega t}], \tag{2}$$

where W_j is the complex amplitude of the generalized coordinate. The kinetic energy of the structure is

$$T=\frac{1}{2}\rho_b b\int_0^L h(x)\sum_{j=1}^{N_1}\phi_j\dot{q}_j\sum_{l=1}^{N_1}\phi_l\dot{q}_l\,\mathrm{d}x, \tag{3}$$

where ρ_b is the beam density and $h(x)$ is the thickness of the beam given by

$$h(x)=\begin{cases}h+h_1, x\in[x_{ci}-\Delta/2, x_{ci}+\Delta/2], & i=1,2,\ldots,R,\\ h & \text{otherwise.}\end{cases} \tag{4}$$

Note that h_1 describes the height of the rib above the beam surface shown in Fig. 1(a) and that all ribs are assumed to have the same height. Substituting Eq. (4) into Eq. (3), the kinetic energy can be expressed as

$$T=\frac{1}{2}\rho_b b\sum_{j=1}^{N_1}\sum_{l=1}^{N_1}(\mu_{jl}^{\mathrm{Tr}}+\eta_{jl}^{\mathrm{Tr}})\dot{q}_j\dot{q}_l, \tag{5}$$

where the superscript Tr represents transverse. It is seen from Eq. (5) that each generalized inertia coefficient is comprised of two parts. The term μ_{jl}^{Tr} represents the inertia effects contributed by a uniform beam of thickness h. The term η_{jl}^{Tr} represents the inertia effects contributed by the R rib discontinuities, each of thickness h_1. These inertia terms are

$$\mu_{jl}^{\mathrm{Tr}}=h\int_0^L\phi_j\phi_l\,\mathrm{d}x, \tag{6}$$

and

$$\eta_{jl}^{\mathrm{Tr}} = \sum_{i=1}^{R} h_1 \int_{x_{ci}-\Delta/2}^{x_{ci}+\Delta/2} \phi_j \phi_l \, \mathrm{d}x. \tag{7}$$

The potential energy of the structure is

$$V = \frac{1}{2} E_b \int_0^L I(x) \sum_{j=1}^{N_1} \phi_j'' q_j \sum_{l=1}^{N_1} \phi_l'' q_l \, \mathrm{d}x, \tag{8}$$

where E_b is the Young's modulus of the beam and $I(x)$ is the position-dependent moment of inertia given by

$$I(x) = \frac{1}{12} b h^3(x). \tag{9}$$

Substituting Eq. (9) into Eq. (8), the potential energy can be expressed as

$$V = \frac{1}{2} E_b \sum_{j=1}^{N_1} \sum_{l=1}^{N_1} (\kappa_{jl}^{\mathrm{Tr}} + \beta_{jl}^{\mathrm{Tr}}) q_j q_l. \tag{10}$$

Each generalized stiffness coefficient is also comprised of two parts. Here, $\kappa_{jl}^{\mathrm{Tr}}$ and β_{jl}^{Tr} represent the bending stiffness contributed by the uniform beam and the rib discontinuities, respectively. Note that by neglecting the β_{jl}^{Tr} terms, the rib discontinuities are then only modeled as distributed mass discontinuities through the terms, η_{jl}^{Tr}. The two bending stiffness terms are

$$\kappa_{jl}^{\mathrm{Tr}} = I \int_0^L \phi_j'' \phi_l'' \, \mathrm{d}x, \tag{11}$$

and

$$\beta_{jl}^{\mathrm{Tr}} = \sum_{i=1}^{R} I_1 \int_{x_{ci}-\Delta/2}^{x_{ci}+\Delta/2} \phi_j'' \phi_l'' \, \mathrm{d}x, \tag{12}$$

where

$$I = \frac{1}{12} b h^3, \tag{13}$$

and

$$I_1 = \frac{1}{12} b (3 h_1 h^2 + 3 h h_1^2 + h_1^3). \tag{14}$$

The generalized force is derived by forming the virtual work expression. As shown in Fig. 1(b), the two actuator excitations are assumed to act on the edges of the ribs. Since these two forces will always be equal and opposite, the piezoelectric force pair will simply be referred to as the piezoelectric force in the remainder of this work. The piezoelectric force is assumed to have the form

$$f(x,t) = \mathrm{Re}[F \, \mathrm{e}^{\mathrm{i}\omega t}] \delta(x - x_0), \tag{15}$$

where x_0 is the location of the force and F is the complex amplitude of the force, which will be described in a later section. The virtual work can be expressed as

$$\delta W_e^{\mathrm{T}} = \int_0^L \left\{ \mathrm{Re}[F \, \mathrm{e}^{\mathrm{i}\omega t}][\delta(x - (x_{c1} + \Delta/2)) - \delta(x - (x_{c2} - \Delta/2))] d \sum_{j=1}^{N} \phi_j' \right\} \mathrm{d}x \delta q_j, \tag{16}$$

where d is the moment eccentricity and the $'$ notation is used to denote the spatial derivative with respect to x. The neutral surface of the structure shown in Fig. 1(b) is assumed to be in the exact middle of lower and upper beam surfaces for the uniform portion of the beam. That is, the effect of the ribs on the neutral axis location is neglected in this initial study. Consequently, the eccentricity is the distance between the force and this neutral axis,

given by $d = h/2 + h_1$. Eq. (16) leads to a generalized excitation given by

$$Q_j = \mathrm{Re}[\widehat{Q}_j \, \mathrm{e}^{\mathrm{i}\omega t}], \tag{17}$$

where

$$\widehat{Q}_j = Fd[\phi_j'(x_{c1} + \Delta/2) - \phi_j'(x_{c2} - \Delta/2)]. \tag{18}$$

Substituting the kinetic energy, potential energy, and the generalized force terms into Lagrange's equations, the structural equations of the transverse motion are found to be

$$\rho_b b \sum_{l=1}^{N_1} (\mu_{jl}^{\mathrm{Tr}} + \eta_{jl}^{\mathrm{Tr}}) \ddot{q}_l + E_b \sum_{l=1}^{N_1} (\kappa_{jl}^{\mathrm{Tr}} + \beta_{jl}^{\mathrm{Tr}}) q_l = Q_j, \tag{19}$$

or in matrix form

$$[M^{\mathrm{Tr}}]\{\ddot{q}\} + [K^{\mathrm{Tr}}]\{q\} = \{Q\}. \tag{20}$$

In this work, a modal transformation is used to gain a better understanding of the structural response. To that end, the eigenvalue problem is first solved in order to obtain the mode shapes and natural frequencies. A modal transformation is then used to decouple the system equations into modal equations. In using this approach, the generalized modal coordinates can be solved in the independent modal space.

Through solving the eigenvalue problem, the generalized coordinates q can be expressed as a linear combination of modal coordinates q^m through the transformation

$$q = Sq^m, \tag{21}$$

where S is the modal transformation matrix consisting of the orthonormal eigenvectors and the superscript m refers to modal. The orthogonal modal shape functions of the discontinuous structure can be expressed by the superposition of the Ritz basis functions as

$$\phi_j^m(x) = \sum_{i=1}^{N_1} S(i,j)\phi_i(x). \tag{22}$$

Therefore, the transverse displacement can be expressed in modal space as

$$w(x,t) = \sum_{j=1}^{N_1} \phi_j^m(x) q_j^m(t), \quad 0 \leqslant x \leqslant L. \tag{23}$$

Furthermore, the corresponding generalized force can be transformed into modal space as

$$\widehat{Q}_j^m = Fd[\phi_j^{m'}(x_{c1} + \Delta/2) - \phi_j^{m'}(x_{c2} - \Delta/2)]. \tag{24}$$

Solving the decoupled equations in modal space, the amplitudes of the modal coordinates can be expressed as

$$W_j^m = \frac{Fd[\phi_j^{m'}(x_{c1} + \Delta/2) - \phi_j^{m'}(x_{c2} - \Delta/2)]}{m_{jj}^{\mathrm{Tr}}[(\omega_j^{\mathrm{Tr}})^2 - \omega^2]}, \tag{25}$$

where ω_j^{Tr} represents the resonant frequencies of the transverse vibration, and m_{jj}^{Tr} represents the modal mass for the jth transverse vibration mode. Note that the value of m_{jj}^{Tr} is one since the eigenvectors are orthonormal. Once the modal coefficients W_j^m are calculated, the transverse displacement of the structure can be reconstructed using Eq. (23).

The axial vibration problem for the ribbed beam can be solved using a similar approach. Due to that similarity, only a brief formulation is presented here. The axial displacement of the beam is expressed by an N_2-term Ritz expansion

$$u(x,t) = \sum_{j=1}^{N_2} \psi_j(x)\vartheta_j(t), \quad 0 \leqslant x \leqslant L, \tag{26}$$

where ψ_j are the basis functions which satisfy the axial geometric boundary conditions and ϑ_j are the axial generalized coordinates. The harmonic time dependency of the generalized coordinates are assumed to be

$$\vartheta_j = \mathrm{Re}[U_j \mathrm{e}^{\mathrm{i}\omega t}]. \tag{27}$$

By forming the kinetic energy, potential energy, and the generalized force of the axial vibration, the equations of axial motion can be expressed as

$$\rho_b b \sum_{l=1}^{N_2} (\mu_{jl}^A + \eta_{jl}^A)\ddot{\vartheta}_l + E_b b \sum_{l=1}^{N_2} (\kappa_{jl}^A + \beta_{jl}^A)\vartheta_l = P_j, \tag{28}$$

where the superscript A will be used to denote terms associated with the axial model and P_j is the axial generalized force. The generalized inertia coefficient terms μ_{jl}^A and η_{jl}^A are

$$\mu_{jl}^A = h \int_0^L \psi_j \psi_l \, \mathrm{d}x, \tag{29}$$

and

$$\eta_{jl}^A = \sum_{i=1}^{R} h_1 \int_{x_{ci}-\Delta/2}^{x_{ci}+\Delta/2} \psi_j \psi_l \, \mathrm{d}x. \tag{30}$$

The generalized stiffness coefficient terms κ_{jl}^A and β_{jl}^A are

$$\kappa_{jl}^A = h \int_0^L \psi_j' \psi_l' \, \mathrm{d}x, \tag{31}$$

and

$$\beta_{jl}^A = \sum_{i=1}^{R} h_1 \int_{x_{ci}-\Delta/2}^{x_{ci}+\Delta/2} \psi_j' \psi_l' \, \mathrm{d}x. \tag{32}$$

The complex amplitude of the generalized force term P_j is then

$$\widehat{P}_j = F[\psi_j(x_{c2} - \Delta/2) - \psi_j(x_{c1} - \Delta/2)]. \tag{33}$$

In matrix form, Eq. (28) can be written as

$$[M^A]\{\ddot{\vartheta}\} + [K^A]\{\vartheta\} = \{P\}. \tag{34}$$

Again, a modal analysis can be conducted to calculate the forced response of the axial vibrations. Using a modal transformation, the axial displacement of the beam is expressed in modal coordinate as

$$u(x,t) = \sum_{j=1}^{N_2} \psi_j^m(x)\vartheta_j^m(t), \quad 0 \leqslant x \leqslant L, \tag{35}$$

where again the superscript m represents modal. Following the same procedure as for the transverse vibration, the amplitude of the modal coordinates can be expressed as

$$U_j^m = \frac{F[\psi_j^m(x_{c1} + \Delta/2) - \psi_j^m(x_{c2} - \Delta/2)]}{m_{jj}^A[(\omega_j^A)^2 - \omega^2]}, \tag{36}$$

where ω_j^A represents the resonant frequencies of the axial vibration, and m_{jj}^A represents the modal mass for the jth axial vibration mode with a value of unity. Once the coefficients U_j^m are calculated, the transverse displacement of the structure can be reconstructed using Eq. (35).

It can be seen from Eqs. (25) and (36) that, if the actuation force F is known, the structural transverse and axial dynamic responses can be predicted. In the next section, the resulting actuation force will be calculated by coupling the structural dynamic response and the piezoelectric actuation strain. Recall that one of the goals of this work is to examine the relationship between the voltage applied to the actuator and the resulting structural motion.

2.2. Piezoelectric actuator modeling

Strain in an unconstrained piezoelectric patch with an applied time-varying voltage $v(t)$ is given by

$$\varepsilon_{\mathrm{pe}} = \frac{d_{31} v(t)}{h_{\mathrm{pe}}}, \tag{37}$$

where d_{31} is the piezoelectric strain constant and h_{pe} is the thickness of the piezoelectric patch [1]. For this study, a harmonically varying voltage

$$v(t) = \mathrm{Re}[V\, \mathrm{e}^{\mathrm{i}\omega t}] \tag{38}$$

will be considered. The actual strain in the piezoelectric actuator is

$$\varepsilon = \varepsilon_{\mathrm{pe}} - \varepsilon_b, \tag{39}$$

where ε_b is caused solely by the axial deformation of the structure at the actuator attachment location. The actuator is a thin structure so that ε_b is assumed to be uniformly distributed through the actuator's cross-section. ε_b can be calculated according to

$$\varepsilon_b = \frac{\Delta l}{l_{\mathrm{pe}}}, \tag{40}$$

where l_{pe} is the unstretched length of the piezoelectric actuator and Δl is the axial deformation of the actuator. As denoted in Fig. 1(a), Δl equals the axial displacement between points P_A and P_B. Although this displacement is axial, it results from both the axial and transverse motion of the beam. For linear vibrations, the transverse vibration's contribution to the piezoelectric deformation can be approximated by the product of the rotation angle at the neutral surface and the corresponding moment arm to the connection point between the actuator and rib. Therefore, Δl can be calculated as

$$\Delta l = [w'(x_{c1} + \Delta/2, t) - w'(x_{c2} - \Delta/2, t)]d + [u(x_{c2} - \Delta/2, t) - u(x_{c1} + \Delta/2, t)]. \tag{41}$$

Substituting Eqs. (23) and (35) into Eq. (41), and then substituting Eq. (41) into (40), the structure strain term caused by the beam deflection becomes

$$\varepsilon_b = \frac{\sum_{j=1}^{N_1} [\phi_j^{m'}(x_{c1} + \Delta/2) - \phi_j^{m'}(x_{c2} - \Delta/2)] q_j^m d + \sum_{j=1}^{N_2} [\psi_j^m(x_{c2} - \Delta/2) - \psi_j^m(x_{c1} + \Delta/2)] \vartheta_j^m}{l_{\mathrm{pe}}}. \tag{42}$$

The axial force within the piezoelectric actuator can be found using the relation

$$f = E_{\mathrm{pe}} A_{\mathrm{pe}} \varepsilon, \tag{43}$$

where E_{pe} and A_{pe} are the Young's modulus and cross-section area of the piezoelectric actuator, respectively. Substituting Eqs. (37) and (42) into Eq. (39), and applying Eq. (43), the amplitude of the piezoelectric strain can be determined as

$$\Lambda = \frac{\Lambda_{\mathrm{pe}}}{1 + C}, \tag{44}$$

where Λ and Λ_{pe} are the complex amplitudes of the actual piezoelectric strain ε and the free strain $\varepsilon_{\mathrm{pe}}$ with the relationships

$$\varepsilon = \mathrm{Re}[\Lambda\, \mathrm{e}^{\mathrm{i}\omega t}] \tag{45}$$

and

$$\varepsilon_{\mathrm{pe}} = \mathrm{Re}[\Lambda_{\mathrm{pe}}\, \mathrm{e}^{\mathrm{i}\omega t}]. \tag{46}$$

In Eq. (44), the parameter C is the ratio of the actuator's axial stiffness to the apparent axial stiffness of the structure at the attachment location as seen by the actuator. The stiffness ratio parameter is given by

$$C = \frac{E_{pe}A_{pe}}{l_{pe}}\left\{\sum_{j=1}^{N_1}\frac{\left[\phi_j^{m'}(x_{c1}+\Delta/2)-\phi_j^{m'}(x_{c2}-\Delta/2)\right]^2 d^2}{m_{jj}^{Tr}[(\omega_j^{Tr})^2-\omega^2]}+\sum_{j=1}^{N_2}\frac{\left[\psi_j^{m}(x_{c1}+\Delta/2)-\psi_j^{m}(x_{c2}-\Delta/2)\right]^2}{m_{jj}^{A}[(\omega_j^{A})^2-\omega^2]}\right\}. \quad (47)$$

Note that the Ritz basis functions are unitless and their spatial derivatives have units of m^{-1}. As a result, the stiffness ratio C is non-dimensional. The apparent axial stiffness of the structure at the attachment location as seen by the actuator is defined as the reciprocal of the part in braces in Eq. (47). The apparent axial stiffness of the structure at the attachment location as seen by the actuator will simply be referred to as the apparent structure stiffness in the remainder of this work. The amplitude of the actuation force exerted on the edges of the ribs can be determined by substituting Eqs. (44) and (45) into Eq. (43),

$$F = \frac{E_{pe}A_{pe}(d_{31}/h_{pe})V}{1+C}. \quad (48)$$

It is seen from Eq. (47) that the transverse and axial motions of the structure both contribute to the apparent axial stiffness of the structure at the attachment location. For the dynamic case (input voltage frequency $\omega>0$), the natural frequencies of the axial vibrations are much higher than those of transverse vibrations. Therefore, the effect of the axial vibration on the piezoelectric strain can be neglected. For the static case (static input voltage $\omega=0$), a numerical study is conducted in a later section to illustrate the contributions of the axial vibrations to the bending moments generated by the piezoelectric force. It is also interesting to note that the rib height has an effect on the piezoelectric strain and force. Consider, for example, the case where the modal shape functions are assumed to not change significantly with the rib height. With an increase in the rib height, as seen from Eq. (47), the apparent stiffness decreases and the corresponding C increases due to the increase in eccentricity d. As a result, the piezoelectric actuation strain and force will decrease. As far as the bending moment is concerned, increasing the rib height will increase the moment arm. However, with the piezoelectric force decreasing, there is a tradeoff between the rib height and the actuator-generated moment. Consequently, there is an optimum rib height that maximizes the bending moment. This optimum height will be numerically studied in a later section. When the rib height is reduced to zero, this piezoelectric-structure model reduces to two line forces on the uniform surface of the beam concentrated at the end of the piezoelectric actuator. In that case, the product of the line actuator forces and the half-thickness of the beam are equivalent to bending moments applied at the beam's neutral axis, a result that is similar to prior work [6]. A comparison between the zero-height rib approach and the prior work of Fuller et al. [6] will be presented in a later section.

Eq. (47) implies that the stiffness ratio parameter C is frequency-dependent. When the driving frequency approaches one of the structure's resonance frequencies, the apparent axial stiffness decreases, which causes the stiffness ratio C to increase. Therefore, it is seen from Eq. (48), the piezoelectric force decreases. On the other hand, the structure is difficult to excite when the excitation frequency is close to the structure's anti-resonance frequencies. As a result, the piezoelectric force will be large, as will be explored later. Note that the dynamic force at zero frequency will be referred to as the static force throughout the remainder of this work. This terminology should not be confused with that of previous studies where a static analysis was used to find the relationships for strain.

Once the piezoelectric actuation forces are determined, the structural dynamic response can be predicted using Eqs. (23) and (35). The induced surface strain on the beam can then be found through application of [7]

$$\varepsilon_s(x,t) = -\frac{h(x)}{2}\frac{\partial^2 w(x,t)}{\partial x^2}+\frac{\partial u(x,t)}{\partial x}. \quad (49)$$

In active vibration control problems, piezoelectric actuators are used to provide control inputs in an attempt to reduce the structural vibrations. Although this paper is not about control system design, it is still interesting to analyze the actuation characteristics in the presence of an external disturbance force. That situation is addressed in the next section.

2.3. Actuation force when an external disturbance is present

It can be seen from Eqs. (44), (47), and (48) that the piezoelectric strain and force depend not only on the input excitation voltage, but also on the structure's dynamic response. If the structure also has an external disturbance force, f_p, such as shown in Fig. 1(a), the structural response depends on both the actuator and the disturbance force. Consequently, when the goal is to reduce the vibration level, as in the case of active vibration control, the disturbance force must be considered when determining the voltage level required for a desired level of actuation.

For simplicity, the external disturbance in this work is assumed to be a point force transversely exerted on the beam at the position $x = x_p$, and at the same frequency as the actuator, as shown in Fig. 1(b). The point disturbance is assumed to have the form of

$$f_p(x,t) = \mathrm{Re}[F_p\, \mathrm{e}^{\mathrm{i}\omega t}]\delta(x - x_p). \tag{50}$$

The piezoelectric force can be predicted by following procedures similar to those described in the two earlier sections of this work. That is, the structural kinetic energy and potential energy terms are the same as before. Due to the existence of the external disturbance force, though, the generalized force will be different from the one given by Eq. (18). For the transverse motion, the virtual work done by the actuator and the disturbance force is given by

$$\delta W_e^d = \delta W_e^{\mathrm{Tr}} + \int_0^L f_p \sum_{j=1}^{N_1} \phi_j \,\mathrm{d}x\, \delta q_j, \tag{51}$$

where the superscript d is used to represent the virtual work when an external disturbance is present. Substituting Eqs. (16) and (48) into Eq. (51), the new generalized force for transverse motion is expressed as

$$\widehat{Q}_j^d = Fd[\phi_j^{m'}(x_{c1} + \Delta/2) - \phi_j^{m'}(x_{c2} - \Delta/2)] + F_p\phi_j^m(x_p). \tag{52}$$

By replacing Q_j in Eq. (19) with $\widehat{Q}_j^d$, the equations for transverse motion with a disturbance force are found. Furthermore, replacing $\widehat{Q}_j^m$ with $\widehat{Q}_j^d$, and solving the decoupled modal equations, the modal coordinates can then be expressed as

$$q_j^d = \mathrm{Re}[W_j^d\, \mathrm{e}^{\mathrm{i}\omega t}], \tag{53}$$

where

$$W_j^d = \frac{Fd[\phi_j^{m'}(x_{c1} + \Delta/2) - \phi_j^{m'}(x_{c2} - \Delta/2)] + F_p\phi_j^m(x_p)}{(\omega_j^{\mathrm{Tr}})^2 - \omega^2}. \tag{54}$$

Replacing q_j^m in Eq. (42) with q_j^d expressed in Eq. (53), and then substituting Eq. (42) into the piezoelectric actuator strain expression in Eq. (39), the piezoelectric actuator strain is now expressed as

$$\Lambda' = \frac{\Lambda_{\mathrm{pe}} - \Lambda_d}{1 + C}, \tag{55}$$

where Λ' is the amplitude of piezoelectric strain with the presence of the external disturbance, and Λ_d is the piezoelectric strain amplitude due to the external disturbance force. The term Λ_d is given by

$$\Lambda_d = \frac{F_p d}{l_{\mathrm{pe}}} \sum_{j=1}^{N_1} \frac{\phi_j^m(x_p)[\phi_j^{m'}(x_{c1} + \Delta/2) - \phi_j^{m'}(x_{c2} - \Delta/2)]}{(\omega_j^{\mathrm{Tr}})^2 - \omega^2}. \tag{56}$$

Clearly, the piezoelectric strain depends on both the magnitude and phase of the external disturbance F_p. Replacing Eq. (44) with (55), and together with Eqs. (45) and (46), Eq. (43) can now be written as

$$F' = \frac{E_{\mathrm{pe}}A_{\mathrm{pe}}((d_{31}/h_{\mathrm{pe}})V - \Lambda_d)}{1 + C}. \tag{57}$$

The piezoelectric force, therefore, depends not only on the input voltage V, but also on the external disturbance F_p, as shown through Eqs. (56) and (57). Furthermore, due to the addition of the strain term associated with the external disturbance in Eq. (57), the relationship between the actuation force and the input voltage will be nonlinear. For example, a doubling of the actuation voltage will not necessarily result in a doubling of the actuator force, due to the fact that the response caused by the external disturbance impacts the baseline strain in the actuator, which consequently impacts the actuator's output force. Of course, a doubling of the actuator force will always correspond to a doubling of the structural response due to that force since the structural model is linear. The nonlinear voltage–force relationship will be discussed at length in the next section.

Before proceeding with the numerical results, it is worth noting that even though the external disturbance considered above is treated as a transverse point force, the above approach can also be applied to such disturbances as a point moment, a distributed force, or another piezoelectric actuator. For these other cases, expressions similar to those in Eqs. (56) and (57) can be obtained for the piezoelectric strain and force.

3. Numerical results and discussions

In this section, the response of a simply supported aluminum beam with four rib discontinuities and a piezoelectric actuator spanning two of those ribs is investigated numerically. The non-dimensional stiffness ratio C is first examined for different excitation frequencies and different rib heights. Then, the characteristics of the actuation force are discussed and the frequency-varying dynamic model for the actuator is compared with a constant-valued model by using the beam frequency response and surface strain distribution. Furthermore, the control authority issue is examined by considering different actuator locations.

The length of the beam is $L = 1\,\text{m}$, the width and thickness of the beam are $b = 30\,\text{mm}$ and $h = 8\,\text{mm}$, respectively. The center positions of the ribs are at $x_{c1} = 0.25\,\text{m}$, $x_{c2} = 0.35\,\text{m}$. $x_{c3} = 0.65\,\text{m}$, $x_{c4} = 0.75\,\text{m}$, and the width of the ribs is $\Delta = 0.04\,\text{m}$. The density and Young's modulus of the beam are $\rho_b = 2700\,\text{kg/m}^3$ and $E_b = 70\,\text{GPa}$, respectively. As shown in Fig. 1(a), the piezoelectric actuator is bonded such that it spans the first two ribs with a thickness of $h_{\text{pe}} = 0.5\,\text{mm}$. The material of the piezoelectric actuator is assumed to be PZT-5A, with the properties listed in Table 1.

3.1. Piezoelectric dynamic forces with and without external disturbances

As mentioned earlier, the stiffness ratio C is a critical factor in determining the actuation force. Using Eq. (47), C can be calculated for different excitation frequencies and different rib heights. Fig. 2 shows the stiffness ratio C at different frequencies when the rib height h_1 is equal to the beam thickness h. Note that to obtain a finite response at resonance, a modal damping of 0.02 is assumed and added to Eq. (47). As seen in Fig. 2, at resonant frequencies the magnitude of the stiffness ratio C is large due to the fact that the structure appears soft at the attachment location. On the other hand, when the excitation frequency is close to an anti-resonance frequency, the corresponding C is small, as the structure now appears stiff to the actuator.

At a specific excitation frequency, the stiffness ratio is also related to the structural geometric property of rib height. Fig. 3 shows how the stiffness ratio changes with the ratio of rib height to the beam thickness for three excitation frequencies. As can be seen from the figure, for the three frequencies considered, with the increase of the rib height, the apparent structure axial stiffness decreases, which results in the increase of the stiffness ratio C. Although the natural frequencies vary with rib height, the first three frequencies are close to 18.4, 74.2, and

Table 1
Material properties of the piezoelectric actuator (PZT-5A)

Density (kg/m^3)	Strain Constant (m/V)			Compliance (ms^2/kg)				
	d_{31}	d_{33}	d_{15}	s_{11}^E	s_{12}^E	s_{13}^E	s_{33}^E	s_{44}^E
7750	−1.23e−10	2.89e−10	4.96e−10	1.64e−11	−5.74e−12	−7.22e−12	1.88e−11	4.75e−11

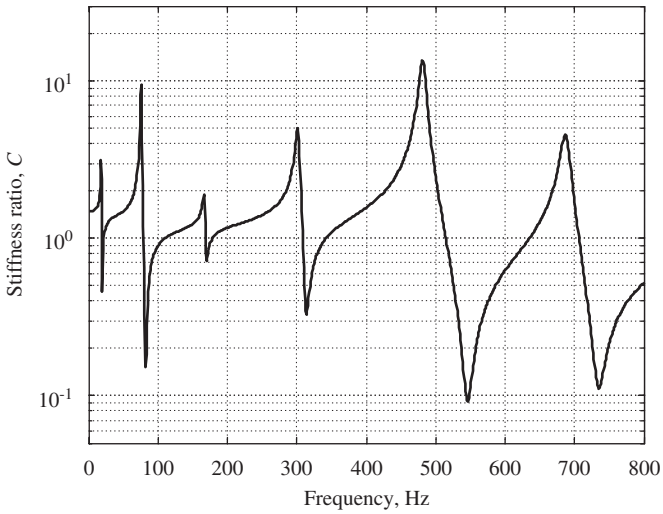

Fig. 2. Magnitude of stiffness ratio C versus excitation frequency.

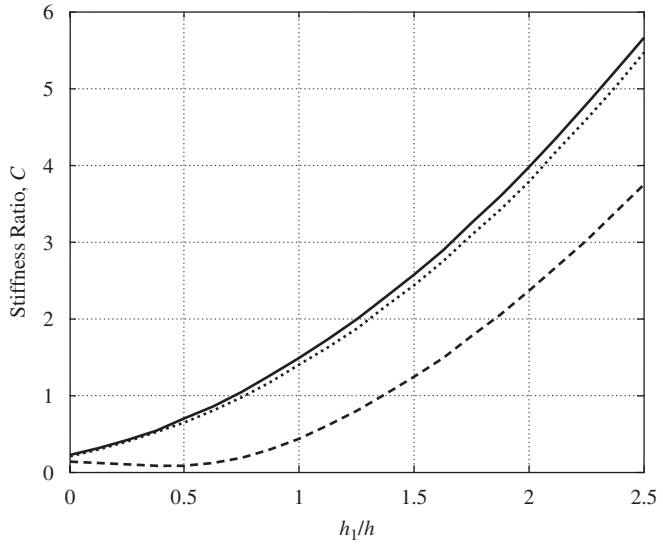

Fig. 3. Magnitude of stiffness ratio C versus rib height ratio at different excitation frequencies: (—) 0 Hz, (- - -) 20 Hz, and (…) 40 Hz.

168.1 Hz, respectively. As h_1 increases from zero to $2h$, the natural frequency variations are within five percent of these nominal values. It is interesting to note from the figure that when the excitation frequency is 40 Hz, which is an off-resonance frequency, the stiffness ratio is very close to that of the static (zero frequency) excitation. When the excitation is close to the anti-resonance frequency (20 Hz), the stiffness ratio is lower, since the structure appears stiffer. In the case of the 20 Hz excitation, there is initially a small decrease in stiffness ratio as the rib height increases, but for h_1/h ratios greater than approximately 0.5, C increases with a trend similar to the 0 and 40 Hz cases.

Under a harmonic input voltage with the magnitude of $V = 10$ V, the dynamic piezoelectric force is computed using Eq. (48), in which no external disturbance is present. The force is then recomputed using Eq. (57) for the same input with an external disturbance at $x_p = 0.8$ m with a magnitude of $F_p = 0.1$ N. The phase of the input voltage is assumed to be the same as that of the disturbance. The magnitude and phase of the resulting piezoelectric force for these two cases are shown in Fig. 4. For comparison purposes, the value of the dynamic force at $\omega = 0$ and without an external disturbance is shown by the horizontal dotted line. As the

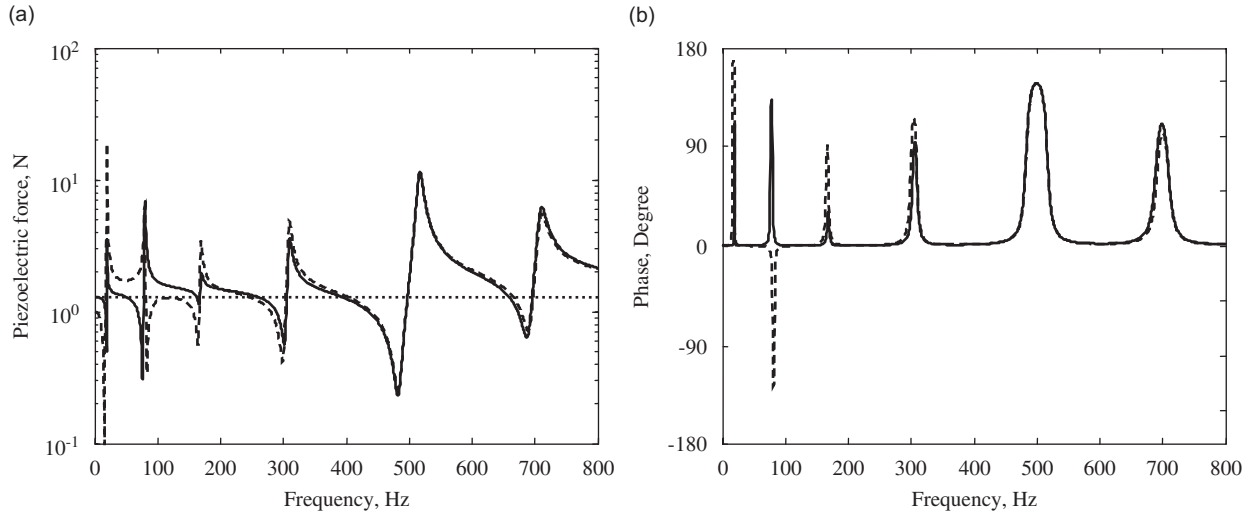

Fig. 4. Piezoelectric forces with input voltage of 10 V: (a) magnitude and (b) phase of piezoelectric forces. (—) without external disturbance, (- - -) with an external disturbance, and (…) static value of the piezoelectric force without external disturbance.

excitation frequency increases, the strain ε_b caused by the deflection of the beam increases for both cases. As a result, the actual piezoelectric strain given by Eq. (39) decreases. Therefore, the force generated by the actuator initially decreases for both cases, as shown in Fig. 4(a). As mentioned in an earlier section, when the excitation frequency approaches the first structural resonance frequency, the structure initially appears soft to the actuator. Therefore, the force generated by the actuator decreases to a local minimum point. As the frequency continues to increase to the first anti-resonance frequency, the structure rapidly becomes stiffer, which results in the increase of the actual piezoelectric force. It is seen from Fig. 4(a) that the associated piezoelectric force passes through the static value and then rapidly increases to a local maximum at the anti-resonance frequency. It can be seen from the phase plot in Fig. 4(b) that at the resonance frequencies, the phase of the piezoelectric force is increased from 0° to 180°; while at the anti-resonance frequencies, the phase of the piezoelectric force is decreased from 180° to 0°. Due to the system damping, between the resonance and anti-resonance frequencies, the phase of the actuation force changes by up to 150° with respect to the input voltage. At off-resonance frequencies, the force and the input voltage are very nearly in-phase.

The effects of the external disturbance point force on the piezoelectric force can be examined by comparing the curves in Fig. 4. The structural response is caused by both the piezoelectric actuator and the external disturbance. As a result, when the excitation frequency is zero, depending on the direction of the external disturbance, the static value of the piezoelectric force will be reduced or increased. In this work, the disturbance force has the same phase as the excitation voltage. As a result, the static value of the piezoelectric force is reduced, as shown in Fig. 4(a). At higher frequencies, it is seen in the figure that with the presence of the external disturbance, the second resonance frequency and anti-resonance frequency are reversed, which results in the $-150°$ phase shift of the piezoelectric force relative to the input voltage. By increasing the input voltage of the piezoelectric actuator to 30 V, the phase of the piezoelectric force between the second resonance and anti-resonance frequency changes back to positive, and the static value of the force increases, as shown in Fig. 5.

Fig. 6 shows the ratio of piezoelectric actuation force when the input voltage is increased from 10 to 30 V. The ratio both with and without the external disturbance force is shown in the figure. Clearly, when there is no external disturbance, the generated piezoelectric force is linearly related to the input voltage, as expressed in Eq. (48). Therefore, the force ratio should be a constant value of three, as shown in Fig. 6. When an external disturbance is present, however, the relationship between the input voltage and the piezoelectric force varies with frequency. It is seen from Fig. 6 that when a disturbance exists, the piezoelectric force ratio will not remain a constant value of three, especially at low frequencies and in the vicinities of the resonance

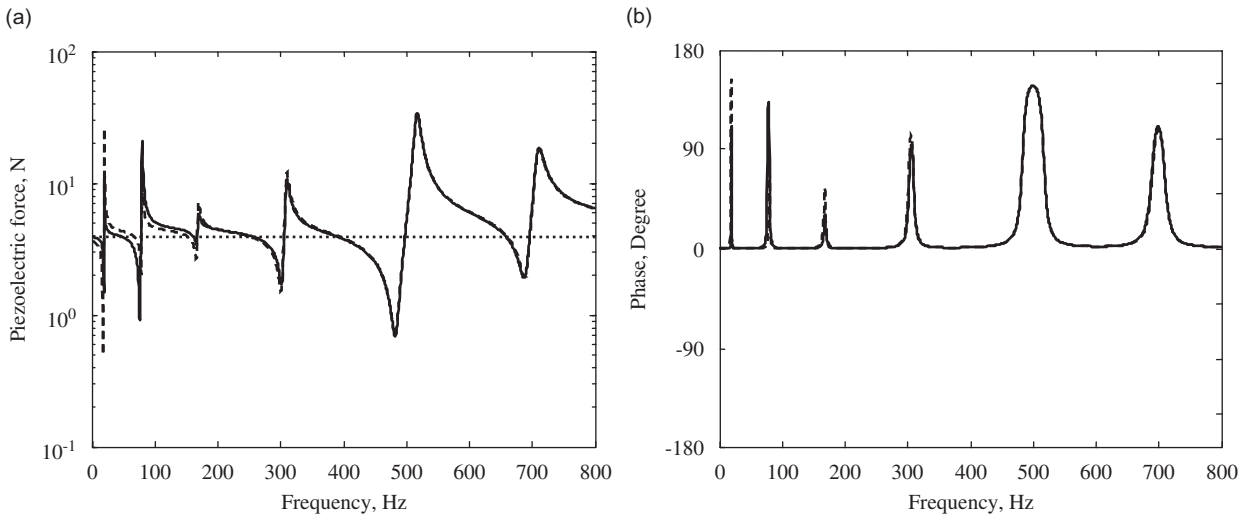

Fig. 5. Piezoelectric forces with input voltage of 30 V: (a) magnitude and (b) phase of piezoelectric forces. (—) without external disturbance, (- - -) with an external disturbance, and (…) static value of the piezoelectric force without external disturbance.

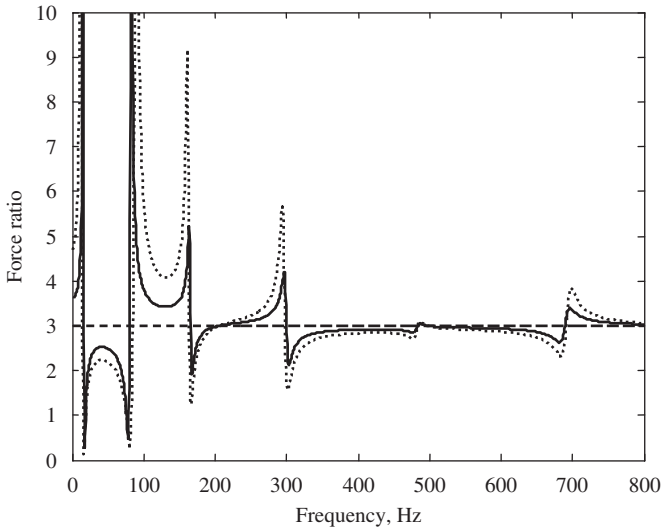

Fig. 6. Piezoelectric force ratio between 30 and 10 V input voltage. (—) with an external disturbance of 0.1 N, (…) with an external disturbance of 0.2 N, and (- - -) without external disturbance.

frequencies. Furthermore, with the increase of the external force from 0.1 to 0.2 N, this nonlinear behavior becomes even more pronounced.

3.2. Static model versus dynamic model

As discussed in Section 3.1, the amplitude of the piezoelectric force is frequency-dependent and varies with the external disturbance. To apply the linear control theories, such as Linear Quadratic Gaussian method, on this model, it is necessary to linearize the nonlinear dynamic model. The linearization approach examined here uses the static value of the piezoelectric force as the frequency-independent amplitude of the harmonic input excitation. In this section, the frequency responses and surface strain responses for the dynamic and static models are compared.

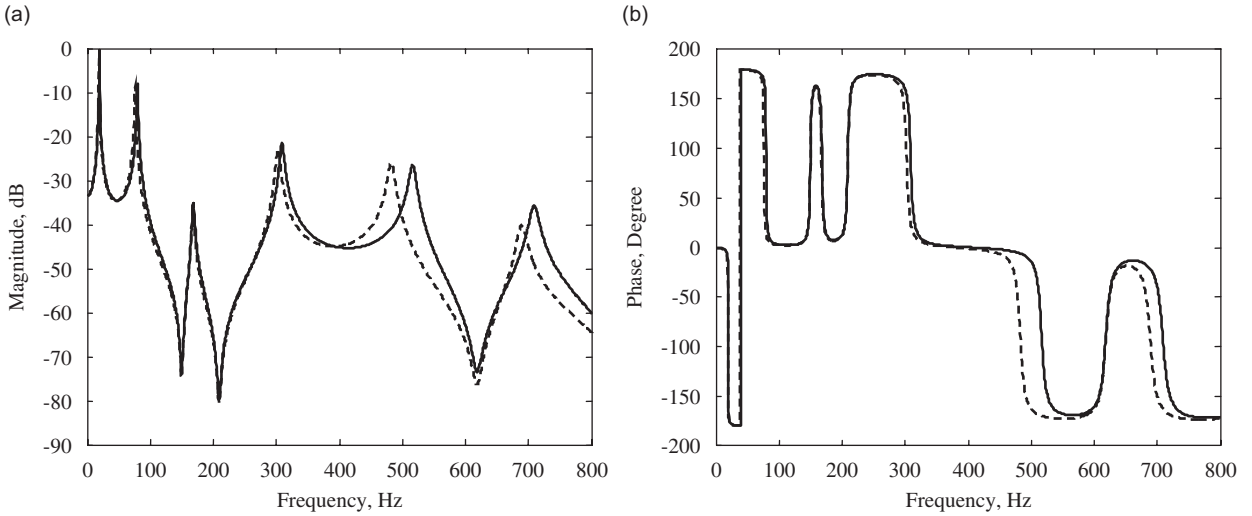

Fig. 7. Frequency-response functions of the static model and dynamic model: (a) magnitude and (b) phase. (—) dynamic model, and (- - -) static model.

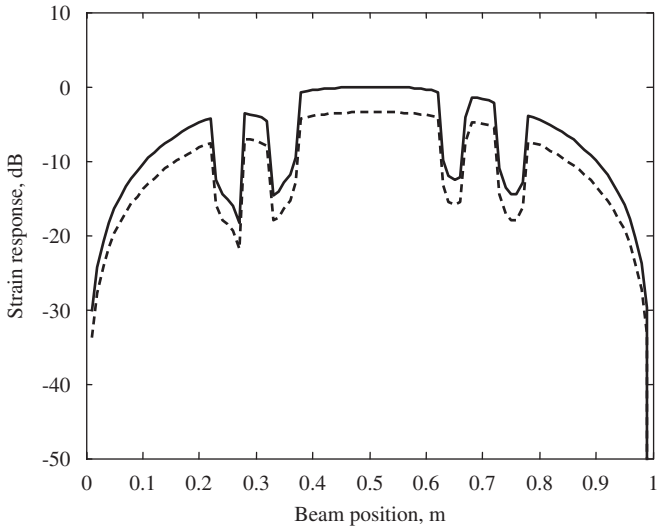

Fig. 8. Beam surface strain distribution at 20 Hz.(—) dynamic model, and (- - -) static model.

The frequency-response functions at an arbitrarily point on the beam $x = 0.65$ m for the two different cases are shown in Fig. 7. Note that in the figure the 0 dB reference is set as the maximum value of the frequency response. It is seen from Fig. 7 that the two models provide generally similar predictions of the beam frequency response, with all significant discrepancies occurring at higher frequencies. As such, the linearized static model can be used to approximate the nonlinear dynamic model at relatively low frequencies, such as near the first several natural frequencies.

The surface strains caused by the structural motions are now calculated at the driving frequencies of 20 and 40 Hz, and shown in Figs. 8 and 9, respectively. Note that in these two figures the 0 dB references are set as the maximum values of the surface strains. In Fig. 8, the surface distributed strain at a frequency just higher than the first natural frequency of the beam is calculated using the dynamic and static models. In Fig. 8, it can be seen that the dynamic model shows larger surface strain at this frequency, which is because the active structure has higher resonant frequencies obtained though the dynamic model than through the static model, as

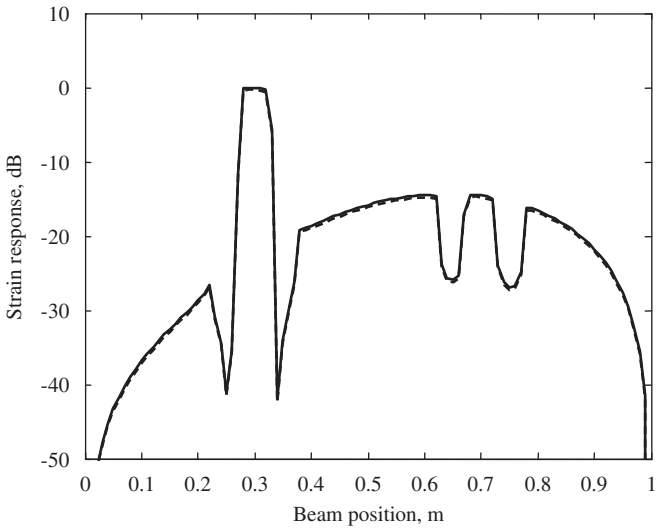

Fig. 9. Beam surface strain distribution at 40 Hz.(—) dynamic model, and (- - -) static model.

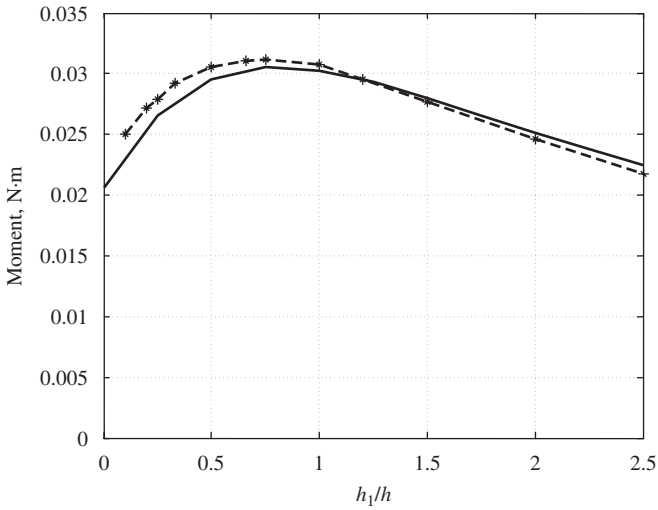

Fig. 10. Generated moment versus the ratio of the rib height to the beam thickness. (—) analytical results, (*) FEM results, and (- - -) linear interpolations of the FEM results.

previously shown in Fig. 7. Fig. 9 shows the surface strain comparisons between the two models at an off-resonance frequency. It is seen in that figure that the two models predict similar strain results.

3.3. Control authority for different actuator configurations

The piezoelectric actuator-induced moments, which determine the input model of the control system can be used to measure the control authority of the actuator for a particular configuration. As mentioned in the first section, the configuration with the actuator spanning the discontinuities will have a different control authority than when the actuator is bonded on the uniform part of the structure. The impact of this control authority on the structure's flexural vibrations will be numerically examined in this section.

By letting the excitation frequency be zero, the static moment M in the beam due to the static actuation force is given by $M = Fd$. Fig. 10 shows the induced moment in the beam with respect to the ratio of the rib

height to the thickness of the beam with an input of 20 V. As mentioned in an earlier section, as far as the bending moment is concerned, increasing the rib height will increase the moment arm, but at the same time, it will also decrease the apparent structure stiffness at the attachment location, resulting in a smaller piezoelectric actuation force. Consequently, there is an optimal rib height that maximizes the bending moment. The induced moment as a function of the ratio h_1/h is shown in Fig. 10. It can be seen in that figure that the optimum rib height is approximately 75% of the beam thickness. With that rib height, the actuator reaches a maximum in terms of structural control authority.

To verify the analytical results, a FE model was developed using ANSYS. In the FE model, a piezoelectric actuator is bonded on two adjacent ribs of a beam structure, and the geometric dimensions of the structure are the same with the analytical model described above. The piezoelectric actuator is modeled with the 3-D coupled-field solid element SOLID5, which has eight nodes with up to six degrees of freedom at each node. The beam structure is modeled with the 3-D structural solid element SOLID45. The generated moments in the structure with an input of 20 V are shown in Fig. 10, superimposed over the earlier analytical results. It is apparent in that figure that the analytical and FE model results match well, with most discrepancies being 5% or less.

The induced moment when the actuator is bonded on the discontinuous side of the beam is now compared with that case when the actuator is bonded on the uniform side of the beam. The induced moments with the actuator bonded on the uniform side of the beam are computed using the model developed by Fuller et al. [6]. A moment ratio, R_m, is defined as the ratio of the moment generated by the actuator spanning the two discontinuities to the moment generated by the actuator bonded on the uniform side of the beam. Fig. 11 shows the moment ratio versus the height ratio of the ribs. It is seen from the figure that when the rib height is zero, there still exists a small difference between the moments computed using the current model and the moments computed using the model developed by Fuller et al. [6]. The reason for this discrepancy is that in their model, the piezoelectric stress is assumed to vary linearly through the cross-section of the piezoelectric actuator. In the current work, however, it is assumed that the piezoelectric stress is uniformly distributed through the actuator cross-section. It can be shown that if there are enough Ritz expansion terms N_1 and N_2 in Eqs. (1) and (26) in the work at hand, and if the piezoelectric stress is assumed to be uniformly distributed through the cross-section of the actuator model given in Ref. [6], the two models will generate similar bending moments at the neutral axis. The assumption of a uniform distribution is based upon the expectation that the piezoelectric actuators will be thin relative to their distance from the neutral axis, particularly when spanning two ribs. As such, any stress variations through the cross-section of the actuator, such as linear variations,

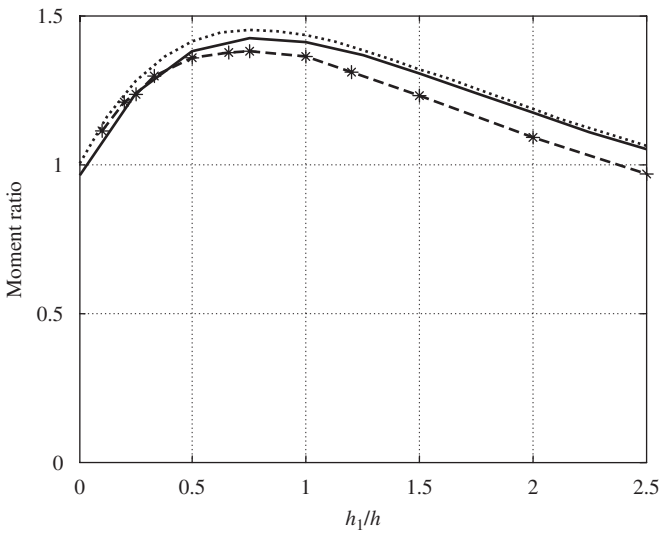

Fig. 11. Moment ratio between the different actuator locations. (—) analytical results when axial motion is considered, (…) analytical results when axial motion is neglected, (*) FEM results, and (- - -) linear interpolations of the FEM results.

would be negligible in comparison to the mean value. When the rib height is about three quarters of the beam thickness, the generated moments from the actuator spanning two adjacent ribs are 42% larger than those when the actuator are put on the uniform side of the beam. As mentioned earlier, it is interesting to examine the contributions of the structure's axial deflection on the piezoelectric force. The analytical results of R_m when the axial deflection of the beam is neglected in the current model are shown as the dotted line in Fig. 11. It is seen that the solid line and dotted line are relatively close, especially when the thickness ratio is high. This result means that when the rib height is relatively large, the axial motion of the structure can be neglected without significant loss of accuracy when considering the bending moment generated on the neutral surface of the structure by the actuator. The above analytical results were validated by the FE results, which are also shown on Fig. 11. Note that in the FE analysis, since this is a 1-D structure, the piezoelectric strain in the y direction is not considered. It is seen from the FE results in Fig. 11, that when the rib height is about three quarters of the beam thickness, the control authority of the actuator spanning two ribs is 38% larger than when the actuator is bonded on the uniform side of the structure.

4. Conclusion

An analytical and numerical study of the excitation of a discontinuous structure with a piezoelectric actuator spanning two adjacent discontinuities is presented. Through numerical examples, it is shown that the piezoelectric force is out of phase with the input voltage when the excitation frequency is close to the structural resonance and anti-resonance frequencies. With the presence of an external disturbance, the linearity between the input voltage and the piezoelectric force will not hold, especially when the actuator is driven at low frequencies and in the vicinities of the resonance frequencies. Approximating the dynamic piezoelectric force with its static value as the frequency-independent amplitude of the harmonic force input can generate relatively good results in structural frequency-response prediction. However, care should be taken at the resonance frequencies as the static model underestimates the resonance frequencies of the active structure. Through an analytical study and FEM study, it is also shown that when the actuator is placed such that it spans two adjacent structural discontinuities, there is a potential for greater control authority over structural vibrations, as compared to the case of the actuator being bonded to the uniform side of the beam.

References

[1] E.F. Crawley, J. de Luis, Use of piezoelectric actuators as elements of intelligent structures, *AIAA Journal* 25 (1987) 1373–1385.
[2] R.L. Clark, C.R. Fuller, A. Wicks, Characterization of multiple piezoelectric actuators for structural excitation, *Journal of the Acoustical Society of America* 90 (1991) 346–357.
[3] E.K. Dimitriadis, C.R. Fuller, C.A. Rogers, Piezoelectric actuators for distributed vibration excitation of thin plate, *Journal of Vibration and Acoustics, Transactions of the ASME* 113 (1991) 100–107.
[4] G.P. Gibbs, C.R. Fuller, Excitation of thin beams using asymmetric piezoelectric actuators, *Journal of the Acoustical Society of America* 92 (1992) 3221–3227.
[5] J. Wang, W.S. Shepard Jr., K.A. Williams, C.B. Gattis, Active vibration control of a plate-like structure with discontinuous boundary conditions, *Smart Materials and Structures* 15 (2006) N51–N60.
[6] C.R. Fuller, S.J. Elliott, P.A. Nelson, *Active Control of Vibration*, Academic Press, New York, 1996.
[7] J. Pan, C.H. Hansen, S.D. Synder, Study of the response of a simply supported beam to excitation by a piezoelectric actuator, *Journal of Intelligent Material Systems and Structures* 3 (1992) 3–16.
[8] O.J. Aldraihem, T. Singh, R.C. Wetherhold, Optimal size and location of piezoelectric actuator/sensors: practical considerations, *Journal of Guidance, Control and Dynamics* 23 (2000) 509–515.
[9] K.G. Webber, K.A. Cunefare, C.S. Lynch, ECLIPSE actuators for control of cylindrical structures, *The International Symposium on Active Control of Sound and Vibration, Active 04*, Williamsburg VA, 2004, Paper A04-031
[10] E.F. Crawley, E.H. Anderson, Detailed models of piezoelectric actuation of beams, *Journal of Intelligent Material Systems and Structures* 1 (1990) 4–25.